Assessing the Influence of Reference Spectra on Synthetic SAM Classification Results

Christoph Hecker, Mark van der Meijde, Harald van der Werff, and Freek D. van der Meer

***Abstract*—Spectral matching algorithms, such as the Spectral Angle Mapper (SAM), utilize the spectral similarity between individual image pixel spectra and a spectral reference library with known components. Here, we illustrate and quantify the effects that different sources of reference libraries have on SAM classification results. Synthetic images of three mineral endmembers were classified by using reference libraries derived from airborne hyperspectral imagery, ground spectra (Portable Infrared Mineral Analyser), and from a standard library (United States Geologic Survey). Results show that the source of the reference library strongly influences the classification results if all available wavelengths are used. This effect can be partially neutralized by using appropriate preprocessing methods. Two different types of spectral subsetting of the data, two types of continuum removal, and a combination thereof were tested. Best results were achieved by using a feature subset (i.e., limiting the input wavelengths to the diagnostic absorption features). This increased the average classification accuracy from 74% to 95% (ground spectral library) and from 68% to 94% (standard library).**

***Index Terms*—Image classification, infrared spectroscopy, spectral analysis, Spectral Angle Mapper (SAM), spectral library, spectral similarity measure.**

I. Introduction

In order to classify remote-sensing images into one or several spectral classes, various algorithms are routinely used. These spectral matching algorithms utilize the spectral similarity between individual image pixel spectra and a spectral library with known components. One of the most popular algorithms is the Spectral Angle Mapper (SAM) which was introduced to the remote-sensing community already 15 years ago [1]. Since then, SAM has extensively been used for classification of hyperspectral as well as multispectral data sets in application fields varying from earth sciences [2]–[4] and vegetation research [5], [6] to urban [7] and planetary [8] studies. Its ease of use, indifference to illumination variations as well as the fact that it is available in most off-the-shelf image processing, have made it the classifier of choice for many research and production projects.

As with any other matching or classification algorithm, using SAM not only has benefits but also disadvantages. One of SAM's weaknesses is its dependence on an overall spectral fit. Rather than looking at the shape of individual absorption features, the spectral angle is an average fit over the entire spectral range (or a subset of it) of the data set that is used in the classifications. This may include nondiagnostic parts of the spectrum as well as spectral trends (continuum) that influence the absorption depth as well as position of superimposed features [9]. SAM's insensitivity to illumination differences also entails that it neglects albedo information, [4], [10] which other classification algorithms can make use of [2]. SAM performance is also susceptible to additive effects, general tilting, and wavelength shifts in the spectra.

With that in mind, it can be questioned how much a SAM classification is influenced by the spectral range and reference spectra used. These reference spectra are compared to the individual image pixel spectra and are ultimately responsible for the spectral match (or mismatch) in the data set. The reference spectra can be extracted from three different sources: from ground spectra on samples from the study area, from published standard spectral libraries, or from the image to be classified itself [1].

The objective of this paper is twofold: 1) to illustrate and quantify the effects that different sources of reference spectra have on SAM classification results and 2) to test a number of preprocessing methods and assessed how far these methods can neutralize the influence of different reference sources. To illustrate this, synthetic images were created out of three image derived endmember spectra and their intermediate mixtures. As an example, the minerals illite, alunite, and kaolinite were chosen. These minerals are abundant worldwide in soils and rock units alike and commonly occur together. Alunite and kaolinite are also economically interesting as industrial minerals and as indicators for often gold-bearing epithermal alteration systems [11], [12]. All three minerals show distinct, yet spectrally related absorption features in the short-wave infrared (SWIR) due to vibrational processes involving the aluminum-hydroxyl groups in the mineral structure [13]. Hence, they are challenging to separate in mixtures and small spectral changes can lead to distinct noticeable classification discrepancies. For SAM classification reference libraries, we used spectra derived from airborne hyperspectral imagery (HyMap), ground spectra [Portable Infrared Mineral Analyser (PIMA II)] and from a standard spectral library [United States Geologic Survey (USGS)].

II. Methodology

A. SAM

SAM is a spectral similarity measure where two spectra are compared with each other and a level of spectral similarity is

Manuscript received January 21, 2008; revised April 3, 2008. Current version published November 26, 2008.

C. Hecker, M. van der Meijde, and H. van der Werff are with the International Institute for Geo-Information Science and Earth Observation, 7500 AA Enschede, The Netherlands (e-mail: hecker@itc.nl; vandermeijde@itc.nl; vdwerff@itc.nl).

F. D. van der Meer is with the International Institute for Geo-Information Science and Earth Observation, 7500 AA Enschede, The Netherlands and also with the Department of Physical Geography, Utrecht University, 3508 TC Utrecht, The Netherlands (e-mail: vdmeer@itc.nl).

Digital Object Identifier 10.1109/TGRS.2008.2001035

measured. The spectral angle between two spectra is calculated by taking the arccosine of the dot product of the two spectral vectors [1]

$$\mathrm{SA} = \arccos\left(\frac{\vec{t} \bullet \vec{r}}{\|\vec{t}\| \bullet \|\vec{r}\|}\right) \tag{1}$$

where SA is the spectral angle in radians between the test spectrum t and the reference spectrum r. A small angle between the two vectors shows that the two spectra closely match each other, while a large angle represents large differences and, therefore, a poor match.

Since SAM compares two spectra as n-dimensional vectors, only the directions of the vectors are important, not their length. This has the effect that multiplicative effects or gain differences in data sets do not influence the resulting spectral angle. This makes the SAM a similarity measure that is insensitive to topographic illumination variations or general albedo differences which often still occur in remote-sensing data sets as well as in spectra of differently calibrated field and laboratory spectrometers. Additive effects (i.e., positive or negative reflectance value shifts for the entire spectrum) do pose a problem for the SAM algorithm. They create spectra that have absorption feature depths which are not proportional to the overall albedo of the spectrum. This can cause a poor match between test and reference spectrum, although the shape may be identical and only the absorption depth is out of proportion. A typical additive effect in HyMap is atmospheric scattering, which can cause problems with a spectral angle classification if the effect is not properly compensated for during the atmospheric correction. A third important characteristic of SAM is that the resulting SA is merely a single number, an "average" disagreement between the test and reference spectra over the entire spectral range. By looking at the resulting SA number, one cannot know whether the principal contributing factor to the spectral angle was a mismatch in the distinct absorption feature of this class or whether the entire spectrum had a slight mismatch in all bands. Both cases can lead to a spectral angle in a similar range although the latter case may perfectly fit the distinct absorption feature and gets the total SA from small mismatches in each band that are counted together. An example of a general trend that can cause an SA misfit is difference in tilt for the test and reference spectra. Small tilt differences in spectra can be caused by various spectrometers used to record them, by samples impurities (e.g., mixed field samples versus pure standard library spectrum) or can be due to limitations in the atmospheric absorption compensation in ground and image spectra. In order to compare the influence of variable reference sources on classification results, three reference libraries were created from the following data sets: airborne HyMap, ground spectra, and standard spectral library.

B. Spectral Libraries

1) Image Derived Library: In order to build a reference library from image derived spectra, we used a HyMap [14] hyperspectral image data set, which was acquired over the Rodalquilar gold mining area in southeastern Spain. This data take formed part of the HyEurope2004 acquisition campaign coordinated by the German Aerospace Center (DLR) and HyVista Corporation, Australia. The HyMap data used in this paper were acquired on May 18, 2004 in an East to West oriented flight line. Swath width is approximately 2.5 km with a nominal pixel size of 4 m. Adjustment of the HyMap imagery from radiance at sensor to reflectance values was done at DLR and included a geometric correction with PARGE and ATCOR4 with atmospheric/topographic correction [15]. Preprocessing included a vegetation and water mask (based on a preliminary classification), spatial subsetting to the main study area and spectral subsetting to HyMap bands 59–125 (1.30–2.47 μm). By means of this spectral subsetting, we matched the range of the PIMA II field spectrometer and excluded the rather noisy band 126 of the HyMap sensor. The preprocessed HyMap scene was used to extract endmember spectra from the image data themselves. A pixel purity index [16] and convex geometry concepts [17] were used to extract spectrally distinct endmembers. The resulting 16 endmembers were screened and merged where duplicates occurred and the three mineral spectra of interest (illite, alunite, and kaolinite) were stored in the image derived reference library [Fig. 1(a)], which we will call "image library" as of this point forward.

2) Ground Spectral Library: For the purpose of building a reference library with ground spectra, rock samples had been collected in the same area as the HyMap scene. Due to scale differences, "pure" spectra in HyMap and in the field do not match and the endmembers do not necessarily come from exactly the same location. Since samples and imagery come from the same general area, the composition of the individual minerals can be assumed to be comparable to those measured with the HyMap imagery. A PIMA II spectrometer from Integrated Spectronics was used to measure shortwave infrared spectra of these field samples under laboratory conditions. The spectra were acquired in the range of 1.3–2.5 μm with a spectral resolution of about 7 nm. A total of 300 spectra were spectrally analyzed and visually verified in order to find pure endmember spectra of the three minerals of interest. All pure spectra were averaged per mineral and spectrally resampled to match the wavelengths and spectral resolution of the HyMap image data. The resulting three reference spectra were stored in the ground spectra derived reference library [Fig. 1(b)], hereafter referred to as "ground spectral library."

3) Standard Library: The third reference library was created by using spectra from an existing standard spectral library of the USGS [18]. These standard libraries are measured in the laboratory under ideal conditions. Most spectra are measured on monomineralic pure samples. The purity is tested by using other analytical methods such as X-ray diffraction or microprobe analysis [18].

All three minerals of interest can display variations in their composition and mineralogic structure. These variations in turn influence the reflectance spectra of the minerals and can cause wavelength shifts of absorption features as well as influence the width of a feature. In order to allow comparison with the spectra recorded in the field area, we decided to pick the one spectrum per mineral from the vast selection in the USGS Spectral Library that matched the PIMA II spectra closest in

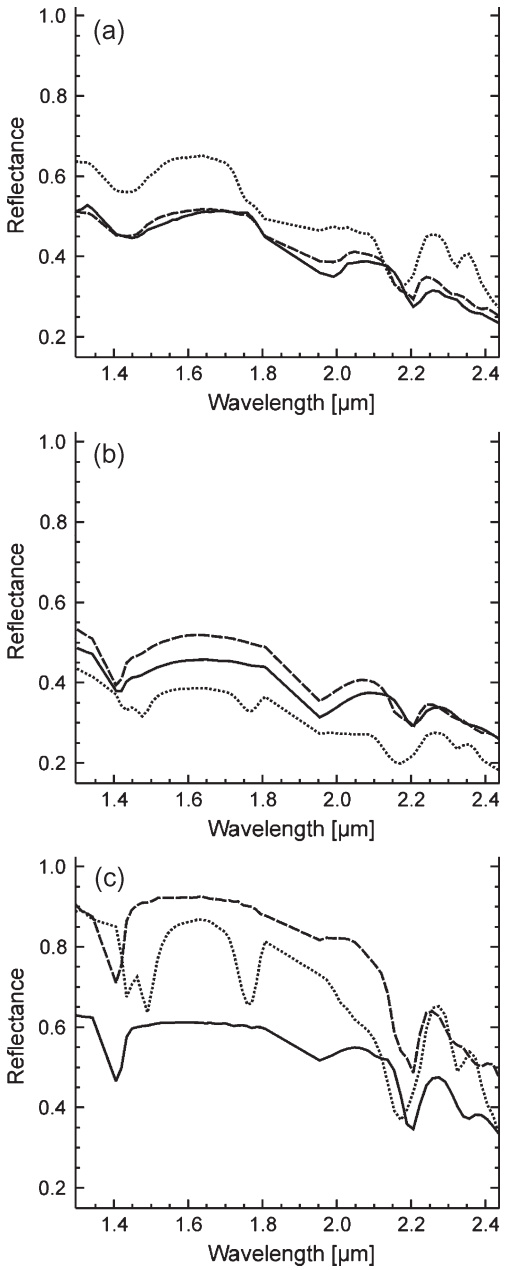

Fig. 1. Spectral reference libraries used in this paper. (a) Image library (from HyMap). (b) Ground spectral library (from PIMA II). (c) Standard library (from USGS). Ground spectral and standard libraries are spectrally resampled to band positions of HyMap sensor. Mineral spectra depicted are from (solid) illite, (dotted) alunite, and (dashed) kaolinite.

terms of absorption feature position and absolute reflectance values (Table I). Spectra were spectrally resampled to match the wavelengths and spectral resolution of the HyMap image data. The resulting three reference spectra were stored in the standard USGS spectral library derived reference library [Fig. 1(c)], hereafter referred to as "standard library."

C. Synthetic Data

For illustrating the classification results and the effect of preprocessing steps in a "controlled" environment, a synthetic data set was created. We opted for the shape of a simple equilateral triangle that represents a classic ternary mixture diagram

TABLE I
SPECTRAL LIBRARY CODES OF SPECTRA USED IN THE "STANDARD LIBRARY"

Mineral Name	USGS Spectral Library Code
Illite	illite4.spc Illite IL101 (2M2)
Alunite	alunite2.spc Alunite GDS83 Na63
Kaolinite	kaolini3.spc Kaolinite KGa-2 (pxyl)

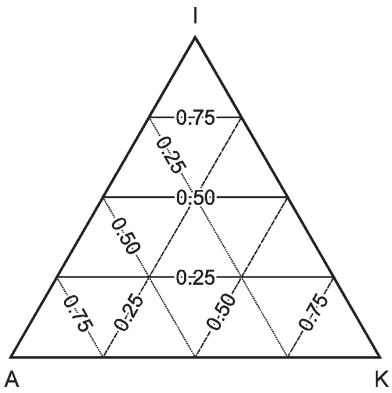

Fig. 2. Ternary mixture diagram for synthetic data set. Contours of mixture fractions are shown for (solid) illite, (dotted) alunite, and (dashed) kaolinite.

(Fig. 2). Each corner represents one of the three endmembers in a pure state. Along each side of the triangle mixtures of two endmembers are located, while the endmember of the opposite corner is not included in the mix. Any point in the interior of the triangle is a mixture of all three endmembers with the mixture fractions depending on the location of the individual pixel. The center of gravity of the equilateral triangle represents the spectral mixture of even amounts of the three endmembers. In order to create a representative spectrum for each pixel in the ternary mixture diagram, we decided to apply a simple linear mixture model by using

$$R_{\mathrm{mix}}(\lambda) = \sum_{i=1}^{3} f_i * R_i(\lambda) \tag{2}$$

where R_i is the spectral reflectance of the pure endmember, f is the fraction in the mixture, and R_{mix} is the resulting linearly mixed spectrum. The three spectra from the image library were used as pure endmember spectra, thus producing a synthetic HyMap-like data set of illite, alunite, and kaolinite mixtures.

D. Enhancement Procedures

Several existing preprocessing procedures were applied to the synthetic data set, in order to test the procedures' potential reducing the influence of reference source data and enhancing the classification results. We tested two different ways of spectrally subsetting the data, two types of continuum removal, and a combination thereof. After this step, the original data set and the enhanced data set were SAM classified with identical settings and the results compared. An overview of the enhancement procedures is given in Table II.

1) Subset: In order to exclude wavelengths that are not characteristic for the endmembers used in this paper, we spectrally

TABLE II
OVERVIEW ON DIFFERENT PREPROCESSING METHODS AND THEIR PARAMETERS. SPECTRAL RANGES IN FEATURE SUBSET ARE GIVEN FOR MINERALS ILLITE (I), ALUNITE (A), AND KAOLINITE (K)

Pre-processing Method	Spectral Range used	Continuum removal	User interaction level	Reasoning
Standard Range	1.30 – 2.47 μm	None	None	Spectral range of PIMA instrument
Subset	2.01 – 2.47 μm	None	Low	Spectral subset to SWIR to focus on general diagnostic region for minerals
Hull Subtraction	2.01 – 2.47 μm	Hull Subtraction	Low	Two types of continuum removal. Reduces effect of general trends in spectra and enhances diagnostic absorption features
Hull Quotient	2.01 – 2.47 μm	Hull Quotient	Low	
Feature Subset	I 2.14 – 2.27 μm A 2.08 – 2.26 μm K 2.10 – 2.26 μm	None	High	Spectral subset chosen for each mineral individually, based on exact position of its diagnostic absorption feature
HQ and FSs		Hull Quotient	High	Combination of hull quotient and Feature Subset pre-processing

subset the data. The idea behind the subsetting is to only include the spectral range with the diagnostic absorption features, which focuses the similarity measure on the spectrally interesting variations in the SWIR [19]. It avoids situations where the SAM results are mainly influenced by dissimilarities in areas that are not relevant for characterizing the endmembers and separating them from each other. Expert knowledge is necessary in order to decide the "characteristic wavelength range" for a given set of spectral classes. While the original synthetic data set has a spatial range of 1.30–2.47 μm, our subset includes HyMap bands 98–125 (2.01–2.47 μm).

2) Continuum Removal: The second enhancement method that was tested was continuum removal, where absorption features and their depth are compared with each other from a common baseline [20]. The idea behind continuum removal is that it eliminates general spectral trends (such as sloping spectra) and focuses on the absorption features superimposed on the general trend.

We chose a baseline or continuum in the form of a convex hull fitted over the top of the spectrum in short, linear segments, which connect local maxima. Other possibilities to define the hull exist (e.g., cubic spline functions) but they result in similar outcomes [9]. Given that the results depend on the starting points of the convex hull, and through that on the spectral range of the data set, we decided to apply continuum removal to the 2.01–2.47 μm subset. This is also the range with the characteristic absorption spectra which we would like to compare. Two types of continuum removal were calculated and the results compared.

Hull subtraction: In what we refer to as "hull subtraction," the corrected reflectance values are determined by subtracting the hull difference from 1.0 (Fig. 3)

$$R_{\mathrm{HS}}(\lambda) = 1.0 - [R_{\mathrm{S}}(\lambda) - R_{\mathrm{H}}(\lambda)] \tag{3}$$

where R_{S} is the original spectral reflectance, R_{H} is the level of the hull, and R_{HS} the resulting hull subtraction corrected spectral reflectance.

Hull quotient: In what we refer to as "hull quotient," the corrected reflectance values are determined by dividing the hull into the spectrum (Fig. 3)

$$R_{\mathrm{HQ}}(\lambda) = \frac{R_{\mathrm{S}}(\lambda)}{R_{\mathrm{H}}(\lambda)} \tag{4}$$

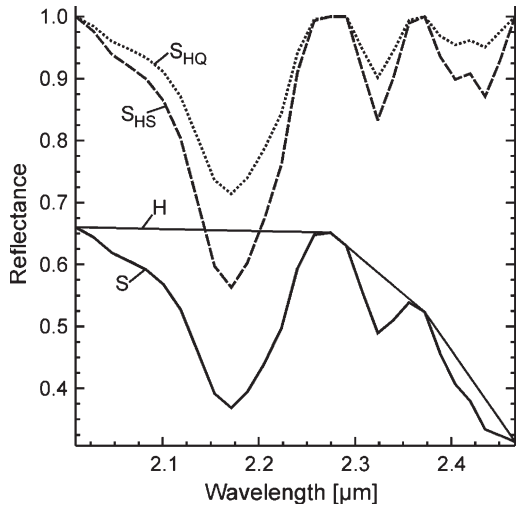

Fig. 3. Effect of hull subtraction versus hull quotient preprocessing on spectra. Original spectrum (S) with its convex hull (H) and the resulting hull subtraction (S_{HS}) and hull quotient (S_{HQ}) corrected spectra.

where R_{S} is the original spectral reflectance, R_{H} is the level of the hull, and R_{HQ} the resulting, hull quotient corrected spectral reflectance. Hull quotient is the continuum removal as implemented in ENVI 4.4 [21].

3) Feature Subset: Under "feature subset," we define a spectral subsetting method that optimizes the spectral range to individual absorption features in the reference classes. The ranges can be varied for each reference class and may also contain several subranges to cover multiple absorption features in the data. While choosing a generic spectral subset for all classes focuses the SAM on generally interesting areas in the spectrum, the feature subset does so for individual absorption features. By this means, we can exclude all but the diagnostic ranges in a mineral spectrum. This sort of subsetting for SAM has previously been suggested by [1]. Nevertheless, in practice, it has not been applied much since then. This may be a consequence of the need for expert interaction in defining these ranges for the individual spectral reference classes.

Choosing feature subset ranges for this paper is rather delicate. The three minerals of interest were partially chosen because they have a main absorption feature at a similar wavelength around 2.2 μm. Hence, the feature subsets for the

three reference minerals show nearly the same range. A single subrange was chosen on the primary absorption feature and includes the shoulders on both sides. The ranges used for the reference spectra are shown in Table II.

4) Hull Quotient and Feature Subset: Results of the techniques described above (as we show below) showed that hull quotient and feature subset preprocessing reduce the influence of the reference spectra source on classification results. As a last preprocessing technique, the two steps were combined to test if this would further improve the results. Since continuum removal depends on the range selected, all three spectra were continuum removed via hull quotient based on the common 2.01–2.47 μm subset range in a first step. Only then they were subset to their individual absorption feature range listed in Table II.

E. Classification

The synthetic data set was classified by matching it to the image library, the ground spectral library, and the standard library. Since SAM can be applied to individual classes, each mineral is treated separately, and class overlaps are not considered. We chose to include the image library as a classification reference although the same spectra had been used as the source for the synthetic image. These image library classification results will define the maximum classification accuracies that can be achieved with SAM on these data sets. All other results can be compared to this "ideal" reference library.

SAM similarity images (or rule images) were calculated for each combination of three reference spectra, three reference libraries, and the various preprocessing steps. To be able to show discrete classification results, the continuous rule images required thresholding: Pixels with rule-image values below the chosen threshold are similar enough to that particular reference spectrum and are assigned to this class, while pixels with larger SA than the threshold are not assigned to this class. Since three endmembers are used, some pixels may score below the threshold of several rule images. This is often dealt with by assigning those doubtful pixels to the rule-image class in which the pixels have the lowest spectral angle value.

Threshold values needed to be determined for each rule image. For this purpose, rule-image histograms were calculated, and the 25th percentile threshold values determined. The choice of the 25th percentile is rather arbitrary. We based it on the fact that 25% of all pixels in the synthetic data set contain mixture fractions of 50% or higher of the endmembers illite, kaolinite, and alunite, respectively. The remaining 25% pixels contain mixtures that are not dominated by any of the three endmembers.

F. Normalization

In order to judge the quality of the classification and quantify the improvements achieved, the result needs to be normalized against a benchmark. For that purpose, we compared each of the classified rule images of the ground spectral library and standard library against the optimal results of the image library. The fraction of pixels that coincided with the "ideal" classification pixels were used as a proxy for classification accuracy

$$\mathrm{Acc}_{\mathrm{mi,rl}} = \frac{N(R_{\mathrm{mi,rl}} \cap R_{\mathrm{mi,ideal}})}{N(R_{\mathrm{mi,rl}})} \tag{5}$$

where $R_{\mathrm{mi,rl}}$ is the classified rule image of a given mineral and reference library, $R_{\mathrm{mi,ideal}}$ is the ideal classification achieved with the image library, and $\mathrm{Acc}_{\mathrm{mi,rl}}$ the resulting accuracy for a given mineral and reference library combination. Hence, the accuracy reported in this paper is never an absolute accuracy that would be achieved in a real world classification. It is rather a percentage of overlap with the optimally achievable classification result of the image library.

III. Results

A. Spectral Libraries

Fig. 1 shows the three reference libraries used in this paper. They differ in absolute reflectance values of their spectra. This is primarily because they were recorded with three different instruments which all have their own radiometric calibration functions. One instrument (image library, i.e., HyMap) is also a passive airborne system that required atmospheric correction of the data. Another major difference is the fact that the spectra in the standard library were measured on pure monomineralic samples. There was no possibility for organic matter or other impurities to reduce reflectance values or for moisture in the sample to influence the reading. As long as the higher reflectance values and deeper absorption features of the standard library are just a question of a different gain factor, SAM results should not be influenced by the discrepancy in reflectance values.

All three minerals possess a primary diagnostic absorption features around 2.2 μm. In all three reference libraries, these features are well developed, with comparable feature shapes and with minima at the same wavelength. In contrast, the absorption depth and even the relative absorption depth varies greatly; while the image library and the ground spectral library have similar absorption depths, the standard library shows much more spectral contrast. Even a gain adjustment (by multiplying with a correction factor to bring the reflectance values into the same range) does not fully "correct" the deeper absorption features of the standard library. This is shown for the mineral alunite in Fig. 4.

Secondary absorption features around 1.45 μm can also be diagnostic for the identification of the minerals of interest. However, in the image library, these features are not distinctly preserved and of identical shape for all three minerals. Fig. 4 shows that the features are close to the 1.4 μm water-absorption feature and may have partially been masked by the lack of atmospheric transmission. In the ground spectral and standard libraries, these features are distinctly preserved even at the same spectral resolution of the hyperspectral image. Both these libraries were recorded with spectrometers with an active light source and with a small distance between instrument and sample. For those reasons, they suffer from less deterioration of the signal close to the water-absorption features. Since two of the

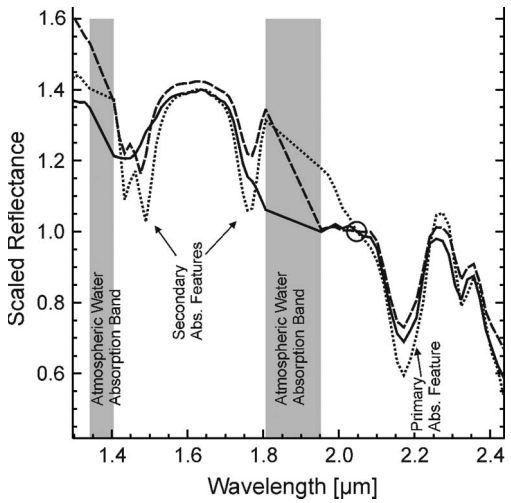

Fig. 4. Alunite spectra of (solid) image library, (dashed) ground spectral library, and (dotted) standard library multiplied with correction factor to bring into the same range (common value of 1.0 at wavelength 2.05 μm; indicated with circle). Alunite spectrum of the standard library still has deeper absorption features after gain correction.

reference libraries contain distinct 1.45 μm absorption features which are not present in the image data, this will inevitably lead to divergence in a spectral matching algorithm if that range is included in the analysis.

For the mineral alunite, we expect another secondary absorption feature around 1.75 μm. It is clearly present in the ground spectral and standard libraries. As with the secondary absorption feature around 1.45 μm previously mentioned, the 1.75 μm feature is barely visible in the image library spectrum, due to its proximity to a water-absorption band.

B. Classification Results

Fig. 5 shows the synthetic images resulting from the SAM matching using a 25th percentile threshold. The locations of the lowest value (lowest spectral angle) in each rule image are indicated as small circles, squares, or triangles (Fig. 5). Where classes spatially overlap the better matching class (i.e., with a smaller SA) is shown on top. Dashed lines indicate the extent of the underlying class. In a final classification, the pixels that pass the threshold criteria of several classes are usually assigned to the class they match best, which in our figures would be the topmost class.

1) Standard Range (1.30–2.47 μm): The classified synthetic images for the three reference libraries are shown in Fig. 5(a).

For the image library as a reference, the corners are properly classified. This is inevitable, as the extreme corner pixel of the synthetic image is always identical to one of the reference spectra in the image library. The classified areas can be approximated by three different shapes: an equilateral triangle, an asymmetric triangle and an ellipse [Fig. 5(a1)].

The alunite-rich corner is classified with equilateral triangle. This indicates that the spectral similarity between alunite and illite is about the same as between alunite and kaolinite. The spectral angles evenly increase out of the alunite corner of the synthetic image and symmetrically along both sides toward the alunite–illite and alunite–kaolinite mixtures.

The shape of the illite class, on the other hand, is that of a strongly asymmetric triangle since alunite is more spectrally distinct from the other two minerals, while kaolinite and illite are more similar. Thus, a mixture of illite and, e.g., 20% kaolinite still has a small spectral angle with the illite reference spectrum (and still falls within the 25th percentile threshold), while illite mixed with a minute alunite component results in a large matching error which immediately falls beyond the classification threshold.

The shape of the pixels in the kaolinite class is that of an ellipse. The elliptical shape and the orientation of its semimajor axis indicate that a mixture of illite and alunite is spectrally similar to the spectrum of kaolinite and causes only a small spectral mismatch. Thus, pixels with less than 50% of kaolinite can still fall within the classification threshold, if the combination of illite with some alunite forms a "kaolinite-like" spectrum. If we look at the reference spectra in Fig. 1(a), this finding is supported by the spectral shapes: In HyMap wavelengths, alunite has an absorption feature centered at 2.17 μm, while that of illite has its midpoint at 2.20 μm. Kaolinite's main feature in that range is a doublet with minima at 2.17 and 2.20. Therefore, the spectrum of a mixture of illite and alunite at the correct proportions is spectrally difficult to distinguish from a pure kaolinite spectrum.

When we classify the synthetic image with the ground spectral library instead, the resulting patterns are changed [Fig. 5(a2)]. The kaolinite class reasonably performs well. The extent of the kaolinite class is slightly less concentrated in the kaolinite corner than for the image library. The alunite class still plots reasonably well in the alunite-rich part of the image, although the extreme corner (i.e., pure alunite) is missed. The lowest rule-image value is scored by a pixel that consists of alunite and about 20% illite. The classification of illite, on the other hand, fails entirely. The classified area almost entirely coincides with the pixels also classified in the kaolinite class, where SA values of in the kaolinite rule image being considerably lower than for illite. Hence, almost no pixels would be classified as illite at all.

The results of using the standard library as reference [Fig. 5(a2)] are similar to those of the ground spectra above. The illite class is again mostly covered by the kaolinite class and would not classify well.

To understand the reason why kaolinite and illite plot in similar places in the synthetic image, we need to consult Fig. 1(a). It shows that spectra of illite and kaolinite in the image library (and hence also in the synthetic data set) are similar for the entire range, except for the 2.2 μm absorption feature. In the reference libraries [Fig. 1(b) and (c)], we can observe that kaolinite shows a steeper general trend (tilt of spectrum from 1.3 to 2.5) in both libraries as compared to illite. If the kaolinite and illite (or mixtures thereof) from the image library are matched against the two reference libraries (ground spectral and standard libraries) kaolinite will score the best match due to the tilt. This is an example where a clear absorption feature match is outweighed by a mediocre general fit over the entire range which leads to this misclassification.

The assessment of the classification success, as described in the methodology, is based on a normalization of the results

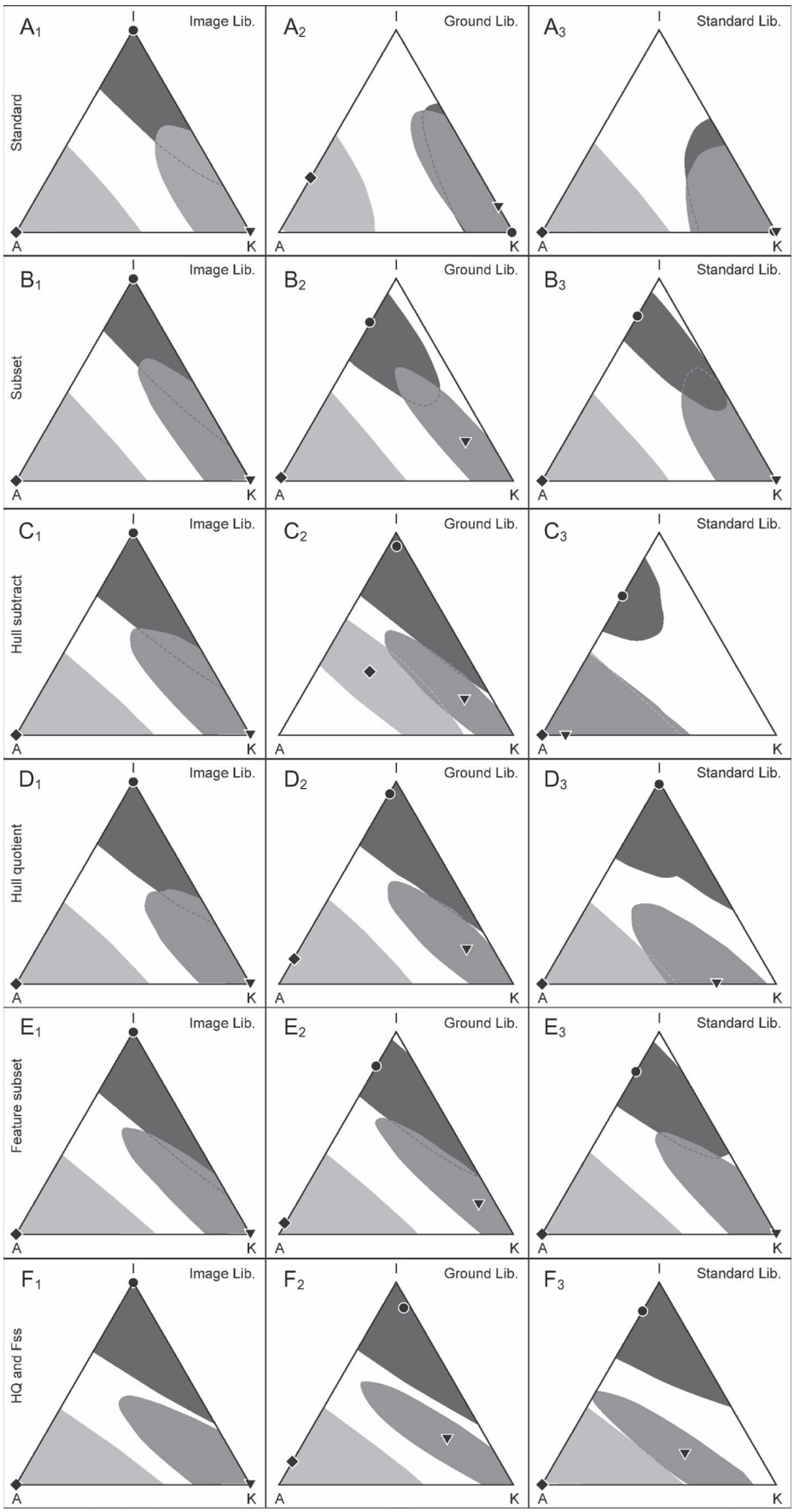

Fig. 5. SAM classification results by reference library and preprocessing method. Shaded areas are those within the 25th percentile threshold for each class rule image. The symbols indicate the location of the smallest spectral angle in the (circle) illite, (square) alunite, and (triangle) kaolinite class.

TABLE III
CLASSIFICATION ACCURACIES FOR VARIOUS PREPROCESSING TECHNIQUES AND REFERENCE LIBRARY (GROUND SPECTRAL LIBRARY AND STANDARD LIBRARY, RESPECTIVELY) ACCURACY VALUES ARE A PERCENTAGE OF OVERLAP WITH THE IDEALLY ACHIEVABLE CLASSIFICATION RESULT (i.e., WITH THE IMAGE LIBRARY AS A REFERENCE)

		Standard Range	Subset	Hull Subtraction	Hull Quotient	Feature Subset	HQ and FSs
Ground spectral library	Illite	38.7%	60.7%	98.8%	98.6%	94.9%	98.9%
	Alunite	91.9%	98.9%	14.3%	100.0%	99.3%	99.1%
	Kaolinite	91.5%	86.6%	82.5%	84.2%	91.2%	84.7%
	Average	74.0%	82.1%	65.2%	94.3%	95.1%	94.2%
Standard library	Illite	23.7%	85.3%	52.0%	89.2%	86.2%	95.0%
	Alunite	99.8%	99.4%	99.6%	99.8%	99.5%	98.6%
	Kaolinite	81.2%	87.0%	00.0%	36.7%	96.9%	37.1%
	Average	68.2%	90.6%	50.6%	75.2%	94.2%	76.9%

with the ideal classification of the image library. These accuracy values are, therefore, a percentage of overlap with the ideally achievable classification result. For alunite and kaolinite classes with ground spectral library, accuracy values of around 92% are reached (Table III). Those for the standard library are 100% and 82%, respectively. Illite, however, reaches a mere 39% with ground spectral library and 24% with standard library. The average accuracy of the three classes together is 74% for ground spectral library and 68% for standard library.

2) Subset (2.01–2.47 μm): After spectrally subsetting the data set to the 2.01–2.47 μm range, the classification was run again. The results are displayed in Fig. 5(b).

For the ground spectral library as a reference, the subsetting has improved the results for the illite class considerably. The class is now appearing in the correct part of the diagram, where illite fractions are high. The lowest spectral angles are along the illite–alunite side of the triangle and still far from the corner where they should be ideally. The corner itself, containing pure illite, is also not included the classification. Overlap between illite and kaolinite classes still exists, although to a much lesser degree than with the standard range. Kaolinite scores the lower absolute SA values than illite and takes priority in a final classification.

Also, for the standard library, the illite class has considerably improved through subsetting. The pure illite corner is again not included in lowest 25% of the illite SA values. Alunite and kaolinite classes are quite similar to image library and ground spectral library results. However, in this case, SA values of kaolinite are larger (more mismatch) than illite. This discrepancy is attributed to mismatches in exact mineral composition between the standard library spectra and the minerals in the study area.

Subsetting the spectra to a range of interest prior to a SAM classification substantially changes the outcome of the classification. Subsetting considerably improved the illite classification accuracy for ground spectra (from 39% to 61%) as well as for the standard (from 24% to 85%) reference libraries (Table III). Average accuracies considerably improved with subsetting, from 74% to 82% (ground spectral library) and from 68% to 91% (standard library).

3) Hull Subtraction: After subsetting and hull subtraction, the results of the image library are similar to the subsetting-only results.

For the ground spectral library, however, we observed mixed results [Fig. 5(c2)]. Illite, which was most troublesome before, has greatly improved. Its shape is now nearly identical to the results of the image library. The elliptic shape of the kaolinite class has become very narrow with the lowest SA values quite far out of the kaolinite corner. Alunite, which was easily classified before, is even worse: Its shape is out of the alunite corner and covers pixels with alunite percentages of 40%–50%, while the alunite richest pixels are not correctly classified.

Classification with hull subtracted standard library as a reference gives the worst results yet [Fig. 5(c3)]: The illite corner is not classified properly, and kaolinite and alunite both plot on top of each other in the alunite corner. Surprisingly, the absolute SA values of the kaolinite rule image are lower than those for alunite. This shows that the alunite-rich corner in the synthetic image matches better with the kaolinite spectrum than with the actual alunite spectrum of the hull-subtracted standard library.

The classification accuracy support these mixed findings as well. As an example, alunite scores accuracies of 14% (ground spectral library) and nearly 100% (standard library). The other minerals also show rather unpredictable results as well, and averaged accuracies are rather low (65% and 51%, respectively).

Keeping the characteristics of SAM in mind, these erratic results are no surprise. By subtracting the spectra from the hull rather than dividing into the hull value, our preprocessing technique contains a nonmultiplicative component. SAM is, however, only insensitive to gain differences. Additive components create an absorption depth misfit between test spectrum and reference spectrum, if they did not have the same general brightness at the start. This can be seen on the example of the alunite class in the ground spectral reference library (Fig. 6). The alunite reference spectrum matches a pure alunite pixel in absorption position and absorption feature shape. The absorption depth, however, is a lot better matched by a mixture of only 45% alunite, and some illite and kaolinite. In this case, the absorption depth outweighs the absorption position with disastrous classification accuracy as a result. In other instances (such as illite reference in the ground spectral library), the absorption position remains dominant and classification results are good. Hence, the classification success is strongly dependent on whether the hull subtraction by coincidence creates absorption features of similar depth in both the test and reference spectra.

4) Hull Quotient: The ground spectral library show much better results with the hull quotient than with hull subtraction.

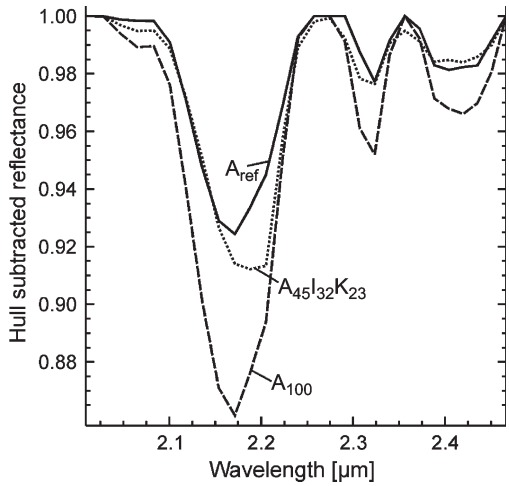

Fig. 6. Influence of hull subtraction and absorption feature depth on matching results. Synthetic test spectra of pure alunite (A_{100}; dashed line) and that of an alunite (45%)—illite (32%)—kaolinite (23%) mixture ($A_{45}I_{32}K_{23}$; dotted line) are shown. The solid line shows the alunite reference spectrum (A_{ref}) of the ground spectral library. Although the absorption feature position and feature shape of the two alunites match very well, the lowest SA is scored by the mixed spectrum ($A_{45}I_{32}K_{23}$). After hull subtraction, its absorption depth is more comparable to that of the reference spectrum.

The hull quotient results are slightly better than for subsetting alone. The pure illite corners are also properly classified, which was not the case in the spectral subset preprocessed image.

In the standard library results, the illite corner is well classified. The kaolinite class, on the other hand, has slightly changed its elliptic shape, and the lowest values are now along the kaolinite–alunite mixture axis.

The classification accuracy (Table III) shows that alunite and illite classify extremely well with accuracies of around 90% or above. Kaolinite, on the contrary, receives rather poor accuracy values; the one for the standard library being as low as 37%. This low value can be explained by the shift of the ellipsoidal class shape as compared to the "ideal" image library classification result which causes a poor overlap. The average accuracies are very high for the ground spectral library (94%) and mediocre for the standard library (75%).

The hull quotient should be the more suitable of the two continuum removal techniques tested in this paper. Since it is a quotient, no additive component is added to the spectra. The relative absorption depth is not tampered with, and the preprocessing technique should have no negative effect on the SAM results. The poor result of the standard library kaolinite reference, however, comes rather as a surprise that requires further discussion. We have shown that the elliptic shapes of the kaolinite class are caused by the spectral similarity between kaolinite and a mixture of illite and alunite. The length of the ellipse's semimajor axis suggests how similar the mix really is to the kaolinite spectrum, while the orientation is an indication on the relative endmember amounts for the best fitting mixture. Due to hull quotient preprocessing, the absorption feature depth of the kaolinite endmembers in the three libraries have undergone slight modifications. Although these changes may be small, they influence the outcome of the classification, in a way that a bit more alunite (which has the deepest absorption feature of all three minerals) is needed to create the best matching mixture of alunite and illite to express kaolinite in the hull quotient case. This is a similar case to the effect shown in Fig. 6.

This rotation of the kaolinite class shape is responsible for the poor overlap between the standard library and "ideal" image library results and, hence, for the low accuracy value of 37%. We believe that for endmembers that cannot be expressed as a linear combination of each other, this problem would not occur. This statement is also supported by the other two mineral endmembers which score excellent hull quotient accuracy results for the ground spectral library as well as the standard library.

5) Feature Subset: For the ground spectral reference library, the classification results with feature subset are very good. The illite class is considerably better as in the general subset case and nearly as good as with the hull quotient preprocessing. Only the extreme corner of the illite is not included in the resulting classification. The kaolinite class is slightly narrower than in the image library but still shows excellent agreement.

The classification output from the standard library also shows excellent results. Alunite is nearly a 100% fit with the image library results. Kaolinite is a slightly broader ellipse but with excellent overlap and illite class also follows the expected shape (although slightly broader and shorter). As with illite in the ground spectral library, the extreme corner is not included, although those are the purest illite pixels.

The classification accuracy (Table III) also supports our interpretation of the classified images. Feature subset preprocessing invariably created very good to excellent results, with average accuracy 95% for ground spectral reference library and 94% for the standard reference library.

6) Feature Subset and Hull Quotient: Feature subset and hull quotient had scored high average accuracies in their individual tests. Both preprocessing steps were combined to test if any further improvement was possible.

When image library was used as a reference library, the resulting classes are well established and separable from each other [Fig. 5(f1)]. The alunite class triangle is somewhat more asymmetric while the illite triangle shows a slight more symmetric shape. The kaolinite class is again elliptic, due to the fact that kaolinite is spectrally similar to an illite–alunite mixture.

For the ground spectral library, the classification results are very good [Fig. 5(f2)]. Illite and alunite classes are nearly identical to the image library results, while the kaolinite class is a somewhat narrower ellipse. The accuracy of the classification is virtually identical to those of the preprocessing with hull quotient alone. Table III shows that illite and alunite score very well, while kaolinite scores lower than expected. The average accuracy reaches 94%. Unlike in the case of feature subsetting alone, all extreme corners are now also classified correctly within the 25th percentile threshold, although the lowest SA values (the best matches) are still not occurring in the extreme corner.

In the standard library, the illite class result is among the best of all preprocessing technique [Fig. 5(f3)]. The extreme corner is classified correctly and the SA minimum is close to its appropriate corner. Alunite again classifies well as with most of the preprocessing techniques. The kaolinite class, however, does not profit from the combined hull quotient and feature subsetting techniques (37%). The same reasoning applies as for

the hull quotient processing. Even with kaolinite scoring poorly, the average accuracy for the standard library still reaches 77%.

C. Normalized Hull Quotient

One way to prevent some of the misclassifications caused by hull quotient preprocessing would be the use of a normalized hull quotient. Spectra are divided into their convex hull and rescaled to the full 0.0–1.0 range. The rescaling avoids the situation where the primary absorption features suffer from differences in absorption depth, since they would all be stretched from 1.0 at the shoulders to 0.0 at the lowest part of the absorption feature. As a consequence, the shape of the absorption feature becomes more powerful in the SAM matching than the absorption depth.

However, absorption depth in itself is an important feature in every classification in order to discriminate major elements in a mixture from accessory materials in tiny proportions. Small amounts of a given endmember in a sample or simply noise in data could create small absorption features that get completely blown out of proportion by a normalized hull quotient procedure. In particular, in small spectral subsets, like the feature subset described above, major absorption feature could be missing and pure noise would be stretched to fit the 0.0–1.0 reflectance range. For those reasons, we do not consider the normalized hull quotient as a workable preprocessing alternative for use in combination with SAM.

IV. Discussion and Conclusion

In this paper, we have shown the negative influence of using different reference libraries for a SAM classification. We used an image library based on HyMap data, the ground spectral library from PIMA II measurements of field samples and the standard library from the published USGS spectral library. Synthetic images were created from the three image library endmembers and their intermediate linear mixtures.

The synthetic data set was matched to all three reference libraries with the SAM algorithm. The results presented show that the source of the reference library strongly influences the classification results. The mismatch of general shape of the reference spectra can diminish (or even overpower) the influence of diagnostic absorption features on the matching result. Differences in the general trend of the spectra can be caused by, e.g., tilting in the general slope of the spectra, differences in absolute reflectance values (additive) or missing features close to water-absorption bands. These effects are often encountered in image data after inadequate data calibration and atmospheric correction. In order to avoid these problems, the reference spectra should ideally be derived from the image data themselves. A main disadvantage is the need for iteratively extracting endmembers from the data set and identifying them correctly, based on the image spectra alone. Local knowledge of what endmembers can be expected in the data or ground spectra of the area can prove very helpful to decide on which and how many endmembers to extract.

As our less preferred alternative, field spectra and standard library spectra can be used. Our results indicate that the field spectra from the same study area performed better than standard spectra from a published library. We believe that the poor results of the standard spectra are related to mismatches in exact mineral composition between the library spectra and the minerals in the field.

We introduced and applied a number of preprocessing methods, and we assessed how far these methods can neutralize the influence of different reference sources. We tested two different types of spectral subsetting the data, two types of continuum removal, and a combination thereof. The spectral subsetting from all bands to a general spectral area of interest immediately increased the average accuracy. The problem of distinct absorption features being overpowered by small discrepancies over a large spectral range is greatly reduced. The second subsetting method, feature subsetting, requires more expert interaction since the subset for each reference spectrum can be chosen individually. The results, however, are even better than with a general subset range for all reference spectra and make the effort more than worthwhile. If expert knowledge is not available or manual interaction in the classification process is not desirable, automatic band selection could be utilized [22]. However, such methods usually require knowledge of the expected spectral endmembers in the image in order to select bands to optimize their separability.

For continuum removal, we first tested a hull subtraction method. While some classes may have slightly increased their accuracy, others classified poorly. The results proved to be extremely unpredictable and unusable in combination with SAM due to the nonmultiplicative component added to the spectra. Our results are based on the limited example of three minerals in a synthetic ternary mixture diagram. The hull quotient method (as well as hull quotient and feature subsets) gave good to excellent classification results for two classes. One class (kaolinite) classified less favorably. Kaolinite's spectral shape is closely linked to the other two classes and can be expressed as a linear combination of the two. We expect that in classification schemes where this is not the case, excellent results will be achieved when the preprocessing includes continuum removal using hull quotients.

Classifying imagery into spectrally distinct classes is not difficult. Problems arise if spectral differences are subtle. In that sense, the outcome of this paper is not restricted to the three-mineral system used here for illustration purposes. We expect that the results are applicable to any study that deals with classes of slight spectral differences and their mixtures, for example, the mapping of tree species in a forest canopy.

The practice of throwing all available bands into a (SAM) classification is still common. The argument that bands that are not containing diagnostic features for the classes of interest can still help with the classification (or at least that they do not harm the results) has herein been proven untrue. Our results clearly show that classification results improve if all disturbing nondiagnostic bands are excluded from the classification.

Acknowledgment

The authors would like to thank the Imaging Spectrometry Group of the DLR and HyVista for the provision and processing

of the HyMap data. The authors would also like to thank the associated editor and three anonymous reviewers for their comments that helped to improve this paper.

REFERENCES

[1] F. A. Kruse, A. B. Lefkoff, J. W. Boardman, K. B. Heidebrecht, A. T. Shapiro, P. J. Barloon, and A. F. H. Goetz, "The spectral image processing system (SIPS)—Interactive visualization and analysis of imaging spectrometer data," *Remote Sens. Environ.*, vol. 44, no. 2/3, pp. 145–163, May/Jun. 1993.

[2] A. P. Crosta, C. Sabine, and J. V. Taranik, "Hydrothermal alteration mapping at bodie, California, using AVIRIS hyperspectral data," *Remote Sens. Environ.*, vol. 65, no. 3, pp. 309–319, Sep. 1998.

[3] G. Ferrier, "Application of imaging spectrometer data in identifying environmental pollution caused by mining at Rodaquilar, Spain," *Remote Sens. Environ.*, vol. 68, no. 2, pp. 125–137, May 1999.

[4] F. van der Meer, "The effectiveness of spectral similarity measures for the analysis of hyperspectral imagery," *Int. J. Appl. Earth Observation Geoinformation*, vol. 8, no. 1, pp. 3–17, Jan. 2006.

[5] J. de Leeuw, H. Jia, L. Yang, X. Liu, K. Schmidt, and A. K. Skidmore, "Comparing accuracy assessments to infer superiority of image classification methods," *Int. J. Remote Sens.*, vol. 27, no. 1, pp. 223–232, Jan. 2006.

[6] J. Zhang, B. Rivard, A. Sanchez-Azofeifa, and K. Castro-Esau, "Intra- and inter-class spectral variability of tropical tree species at La Selva, Costa Rica: Implications for species identification using HYDICE imagery," *Remote Sens. Environ.*, vol. 105, no. 2, pp. 129–141, Nov. 2006.

[7] S. Schiefer, P. Hostert, and A. Damm, "Correcting brightness gradients in hyperspectral data from urban areas," *Remote Sens. Environ.*, vol. 101, no. 1, pp. 25–37, Mar. 2006.

[8] F. Schmidt, S. Doute, and B. Schmitt, "WAVANGLET: An efficient supervised classifier for hyperspectral images," *IEEE Trans. Geosci. Remote Sens.*, vol. 45, no. 5, pp. 1374–1385, May 2007.

[9] R. N. Clark and T. L. Roush, "Reflectance spectroscopy: Quantitative analysis techniques for remote sensing applications," *J. Geophys. Res.*, vol. 89, no. B7, pp. 6329–6340, 1984.

[10] W. H. Bakker and K. S. Schmidt, "Hyperspectral edge filtering for measuring homogeneity of surface cover types," *ISPRS J. Photogramm. Remote Sens.*, vol. 56, no. 4, pp. 246–256, Jul. 2002.

[11] A. Arribas, Jr., C. G. Cunningham, J. J. Rytuba, R. O. Rye, W. C. Kelly, M. H. Podwysocki, E. H. McKee, and R. M. Tosdal, "Geology, geochronology, fluid inclusions, and isotope geochemistry of the Rodalquilar gold alunite deposit, Spain," *Econ. Geol.*, vol. 90, no. 4, pp. 795–822, Jul. 1995.

[12] F. van der Meer, "Indicator kriging applied to absorption band analysis in hyperspectral imagery: A case study from the Rodalquilar epithermal gold mining area, SE Spain," *Int. J. Appl. Earth Observation Geoinformation*, vol. 8, no. 1, pp. 61–72, 2006.

[13] R. N. Clark, "Spectroscopy of rocks and minerals, and principles of spectroscopy," in *Manual of Remote Sensing*, vol. 3, A. N. Rencz, Ed. New York: Wiley, 1999, pp. 3–58.

[14] T. Cocks, R. Jenssen, A. Stewart, I. Wilson, and T. Shields, "The HyMap airborne hyperspectral sensor: The system, calibration and performance," presented at the 1st EARSeL Workshop Imaging Spectroscopy, Zürich, Switzerland, 1998.

[15] D. Schlaepfer, *Remote Sensing Applications–www.rese.ch*, vol. 2007, 2007.

[16] J. W. Boardman, F. A. Kruse, and R. O. Green, "Mapping target signatures via partial unmixing of AVIRIS data," presented at the Summaries, 5th JPL Airborne Earth Science Workshop, San Diego, CA, 1995.

[17] J. W. Boardman, "Automated spectral unmixing of AVIRIS data using convex geometry concepts," presented at the Summaries, 4th JPL Airborne Earth Science Workshop, Pasadena, CA, 1993.

[18] R. N. Clark, G. A. Swayze, A. Gallagher, T. V. V. King, and W. M. Calvin, "The U.S. Geological Survey, digital spectral library: Version 1: 0.2 to 3.0 microns," U.S. Geol. Survey, Reston, VA, Open File Report 93-592, 1993.

[19] A. J. Brown, "Spectral curve fitting for automatic hyperspectral data analysis," *IEEE Trans. Geosci. Remote Sens.*, vol. 44, no. 6, pp. 1601–1608, Jun. 2006.

[20] F. A. Kruse, A. B. Lefkoff, and J. B. Dietz, "Expert system-based mineral mapping in northern Death Valley, California/Nevada, using the airborne visible/infrared imaging spectrometer (AVIRIS)," *Remote Sens. Environ.*, vol. 44, no. 2/3, pp. 309–336, May/Jun. 1993.

[21] *ENVI—Environment for Visualizing Images, Version 4.4.*, ITT Vis. Inf. Solutions, Boulder, CO, 2007.

[22] N. Keshava, "Distance metrics and band selection in hyperspectral processing with applications to material identification and spectral libraries," *IEEE Trans. Geosci. Remote Sens.*, vol. 42, no. 7, pp. 1552–1565, Jul. 2004.

Christoph Hecker was born in 1974. He received the B.Sc. degree in earth sciences and the M.Sc. degree in structural geology and tectonics from the University of Basel, Basel, Switzerland, in 1996 and 1999, respectively, where he studied the structural and tectonic development of the Tasna Nappe in the Swiss Alps.

In 2000-2001, he was with the Belize Audubon Society, Belize City, Belize. Since 2001, he has been with the International Institute for Geo-Information Science and Earth Observation, Enschede, The Netherlands. His research interests include thermal infrared remote sensing, hyperspectral remote sensing, and mid-infrared spectroscopy of rocks and minerals.

Mark van der Meijde was born in 1973. He received the M.Sc. degree in geophysics from Utrecht University, Utrecht, The Netherlands, in 1998, and the Ph.D. degree from the Federal Institute of Technology, Zurich, Switzerland.

In 1997–1998, he was with the Dutch seismological service before he joined the Dutch geological survey in 1998. Since 2003, he has been with the International Institute for Geo-Information Science and Earth Observation, Enschede, The Netherlands. His research is directed toward 3-D geological modeling and integration of surface and subsurface data using remote sensing, geophysics, and geology.

Harald van der Werff was born in 1975. He received the M.Sc. degree in structural geology and the Ph.D. degree from Utrecht University, Utrecht, The Netherlands.

In 1999–2000, he was with the German Aerospace Center, Oberpfaffenhofen, Germany. Since 2001, he has been with the International Institute for Geo-Information Science and Earth Observation, Enschede, The Netherlands. His research interests are hyperspectral remote sensing and advanced image analysis.

Freek D. van der Meer was born in 1966. He received the M.Sc. degree in structural geology and tectonics from the Free University of Amsterdam, Amsterdam, The Netherlands, in 1989, and the Ph.D. degree in remote sensing from Wageningen Agricultural University, Wageningen, The Netherlands, in 1995.

From 1999 to 2005, he was employed as a Part-Time Full Professor of imaging spectrometry with the Faculty of Civil Engineering and Geosciences, Delft University of Technology, Delft, The Netherlands. Currently, he is also the Head of the Department of Earth System Analysis with the International Institute for Geo-Information Science and Earth Observation, Enschede, The Netherlands, and he holds a chair in geologic remote sensing with the Utrecht University. His research is directed toward the use of hyperspectral remote sensing for geological applications with the specific aim of using geostatistical approaches to integrate airborne and field data into geologic models. He is an Associate Editor of the *International Journal of Applied Earth Observation and Geoinformation*, Associate Editor of *Terra Nova*, and Series Editor of the *Remote Sensing and Digital Image Processing Book Series* (Springer-Kluwer).

Prof. van der Meer is past Chairman of the Netherlands Society for Earth Observation and Geoinformatics, Chairman of the special interest group geological remote sensing, and a council member of the European Association of Remote Sensing Laboratories.